

Chapter 2.3.5

LIGHT SCATTERING FROM DENSE POLYMER SYSTEMS

G. Fytas

FORTH/Institute of Electronic Structure and Laser,
P.O. Box 1527,
711 10 Heraklion, Crete,
Greece
and Max Planck Institut für Polymerforschung,
P.O. Box 3148,
D-55021 Mainz,
Germany

SCATTERING IN MICROSCOPIC PHYSICS
AND CHEMICAL PHYSICS

Visible and Near-Visible Light Scattering

Contents

§1	Introduction	1
§2	Physical Principles	1
§3	Experimental Techniques	2
	Photon Correlation Spectroscopy (PCS)	2
	(Time-Domain Analysis)	2
	Fabry–Perot Interferometry (FPI)	3
§4	Dynamic Structure Factor	3
	Diblock Copolymers	3
	Soft Colloids	6
§5	Dynamics of Shape-Persistent Macromolecules	9
§6	Fast Dynamics	11
§7	Outlook	12

(Berne and Pecora, 1976) becomes a selective tool to elucidate the average shape and measure orientation relaxation.

This review surveys recent applications of polarised and depolarised first-order (single) light scattering to interacting nondilute polymer systems. Earlier work and characterisation of dilute polymer solutions for which light scattering is a mature experimental method is described elsewhere (Cummins and Pike, 1974, 1977; Berne and Pecora, 1976; Degiorgio *et al.*, 1980; Chen *et al.*, 1981; Burchard, 1983; Pecora, 1985; Chu, 1991; Schmitz, 1991; Foerster and Schmidt, 1995). The next section presents the basic physical principles of **dynamic light scattering**, and the two main techniques to measure the desired intermediate scattering function $S(q, t)$ are briefly discussed in §3. Following that, the $S(q, t)$ of self-assembled systems (diblock copolymers and soft colloids) and the orientation relaxation function of new shape persistent macromolecules are discussed in §4 and §5, respectively. Finally, we briefly review recent applications of the less frequently used frequency-domain analysis by tandem-Fabry–Perot interferometry to study hypersonic propagation and fast (local) dynamics in disordered systems.

§1. Introduction

The discovery and development of scattering techniques has become extremely beneficial for polymer science. They have fulfilled the central requirement for both space and time resolution since inherent to the nature of this class of soft matter is the presence of a large range of length and time scales (de Gennes, 1979; Doi and Edwards, 1986; Strobl, 1997). While X-ray and neutron scattering (Higgins and Benoit, 1994) provide high magnification, laser light scattering is nowadays unique because of its broad time range, from seconds to picoseconds utilising time- and frequency-domain analysis (Brown, 1993, 1996). The development of new advanced soft materials (Supramolecular Materials, 2000) continuously sets new challenges for dedicated characterisation of their time and space organisation (Pike and Abbiss, 1997). Valuable information on both structure and dynamics can be obtained whenever the scattering wavevector q matches the system characteristic correlation length(s), i.e., $q\xi \sim O(1)$. Further, for systems consisting of nonspherical units anisotropic light scattering

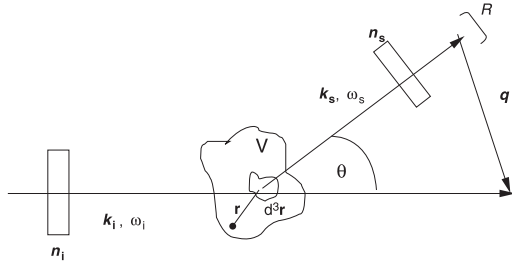
§2. Physical Principles

The scattering geometry with explanation of the symbols is depicted in Fig. 1. The incident laser field $E_i(\mathbf{r}, t) = \mathbf{n}_i E_o \exp(\mathbf{k}_i \mathbf{r} - \omega_o t)$ in a nonabsorbing polarisable medium induces a dipole moment $a(\mathbf{r}, t) E_i(\mathbf{r}, t) d^3 \mathbf{r}$ that scatters at an angle θ , at the detector located at distance R , the field (Chu, 1991; Pike and Abbiss, 1997)

$$E_s(R, \mathbf{q}, t) = A \int_V d^3 \mathbf{r} a(\mathbf{r}, t) e^{i\mathbf{q}\mathbf{r}}, \quad (1)$$

where $A \equiv (E_o \omega_o^2 / c^2 R) \exp[i(\mathbf{k}_s \mathbf{R} - \omega_o t)]$ (c being the speed of light) and $\alpha(\mathbf{r}, t) = \langle \alpha \rangle + \delta\alpha(\mathbf{r}, t)$ with $\delta\alpha(\mathbf{r}, t) = \sum_{j=1}^N \alpha_j(t) [\delta(\mathbf{r} - \mathbf{r}_j(t))]$ being the fluctuations

Figure 1 Laser light of polarisation \mathbf{n}_i with wavevector \mathbf{k}_i and frequency ω_0 is scattered by polarisability fluctuations in the volume V at an angle θ with polarisation \mathbf{n}_s , wavevector \mathbf{k}_s and frequency ω_s . The amplitude scattering wave vector $\mathbf{q} = 2\mathbf{k}_i \sin(\theta/2)$.



of polarisability around the mean value $\langle \alpha \rangle$ in the scattering volume V containing N scatterers. In Fourier space, the component of polarisability density along the initial and final polarisation directions is

$$\delta a_{is}(\mathbf{q}, t) = n_s \left\{ \sum_j a_j(t) \exp[i\mathbf{q} \cdot \mathbf{r}_j(t)] \right\} n_i$$

that leads to

$$E_s(\mathbf{q}, t) = A \delta a_{is}(\mathbf{q}, t) \quad (2)$$

(the trivial term $\langle \alpha \rangle \delta(q)$ was omitted). The scattering event can be envisioned as arising from the diffraction of the light by an effective polarisability grating with periodicity length $2\pi/q$. The measurable quantities are either the time correlation function $C_{is}(\mathbf{q}, t) = \langle E_s(\mathbf{q}, t) E_s(-\mathbf{q}, 0) \rangle$,

$$C_{is}(\mathbf{q}, t) = I_o \left\langle \sum_{ij} a_j(t) a_i(0) \exp i\mathbf{q} \cdot [\mathbf{r}_j(t) - \mathbf{r}_i(0)] \right\rangle \quad (3a)$$

or its spectrum

$$I_{is}(\mathbf{q}, \omega) = (2\pi)^{-1} \int_{-\infty}^{\infty} \exp(-i\omega t) I_{is}(\mathbf{q}, t) dt \quad (3b)$$

where $I_o = \langle E^2 \rangle$ is the incident laser power.

The salient features of Eqs. (3) are: (i) Scattering at finite \mathbf{q} arises from fluctuations of wavelength \mathbf{q}^{-1} , and their correlation in space can modulate the interference (phase) factor expressed by the exponential term in Eq. (3a). (ii) The space organisation, i.e., the structure of the scatterer assembly, can be extracted from the intensity distribution $I(\mathbf{q})$ (Eq. (3a) for $t = 0$) whenever $\mathbf{q} \cdot (\mathbf{r}_j(0) - \mathbf{r}_i(0)) \approx O(1)$. (iii) Translational centre-of-mass and internal motion of the scatterers are reflected in the variation of the interference factor with time. (iv) The signature of overall rotation and internal reorientational motions of nonspherical scatterers is the modulation of the preexponential term of Eq. (3a). In this case, the nonzero off-diagonal components of the polarisability tensor α adds selectivity in the depolarised light scattering component $I_{VH}(\mathbf{q}, t)$. The scattered signal in Eq. (3) therefore

depends on the two main polarisations: $\mathbf{n}_i \cdot \mathbf{n}_s = 1$ for polarised VV scattering and $\mathbf{n}_i \cdot \mathbf{n}_s = 0$ for depolarised VH light scattering; for spherical scatterers the single (Fytas *et al.*, 1996a) depolarised scattering $I_{VH} = 0$.

For **polymers**, it is practical to identify the scattered moiety with the smallest structural unit, i.e., monomer or statistical segment. In this case, Eq. (3a) includes two additional sums over units on different macromolecules each containing N monomers. Obviously, a derivation of analytical expressions from the statistical ensemble of Eqs. (3) would require: (i) validity of the statistical independence of the rotational and translational degree of freedoms, (ii) knowledge of the macromolecular shape to derive the space correlation between the units on the same macromolecule, (iii) motional mechanism for the trajectories of their constituent units, e.g., Rouse, reptation model and (iv) information on the interactions between different macromolecules. It is therefore clear that this constitutes a formidable task. Well-established analytical expressions that provide the basis of polymer characterisation exist for dilute polymer solutions of certain shapes, e.g., random coil, rigid rods, and ellipsoids (Cummins and Pike, 1974, 1977; Berne and Pecora, 1976; Degiorgio *et al.*, 1980; Chen *et al.*, 1981; Burchard, 1983; Pecora, 1985; Chu, 1991; Schmitz, 1991; Foerster and Schmidt, 1995). For dense polymer systems, however, the few cases for which analytical derivations of the scattering function have been proposed will be reviewed in the next sections.

§3. Experimental Techniques

Photon Correlation Spectroscopy (PCS) (Time-Domain Analysis)

In reality square-law detectors measure intensity $I(R, q, t) \equiv |E(R, q, t)|^2$ and hence the measurable quantity by digital correlators is the intensity correlation function $G(q, t) = \langle I(q, t) I(q, 0) \rangle$. In the case of homodyne detection and Gaussian scattered light, the desirable normalised field correlation function $C(q, t)$, (Eq. (3a)) is computed from (Cummins and Pike, 1974, 1977; Chen *et al.*, 1981)

$$G(q, t) = \langle I(q) \rangle^2 \left[1 + f^* |a C^*(q, t)|^2 \right], \quad (4)$$

where $C^*(q, t) \equiv \langle E_s(q, t) E_s(-q, 0) \rangle / \langle |E_s(q, 0)|^2 \rangle$ is the normalised scattered field correlation function, f^* is an experimental instrument factor (which relates the scattered area with the coherence area) calculated by the means of a standard ($f^* = G(q, t \sim 0.1 \mu\text{s}) / \langle I(q) \rangle^2 - 1$), and a is the fraction of the total scattered intensity arising from the fluctuations $\delta a(q, t)$ with correlation times longer than 10^{-7} s. Faster fluctuations can be resolved by frequency-domain analysis (see below). Due to the high-quality experimental data and the

broad time window (10^{-7} – 10^3 s) of PCS, the analysis of $C(q, t) (\equiv \mathbf{a}C^*(q, t))$ can proceed via inverse Laplace transformation (ILT) under the assumption of superposition of exponential decays (Provencher, 1982). The distribution of relaxation times $L(\ln \tau)$ is then extracted from

$$C(q, t) = \int_{-\infty}^{\infty} \exp(-t/\tau) L(\ln \tau) d(\ln \tau). \quad (5)$$

For $\delta\alpha(q, t)$ arising from density fluctuations due to local segmental motions in dense polymer systems, the nonexponential shape of $C(q, t)$ can be represented by the stretched exponential Kohlrausch–Williams–Watts (KWW) function

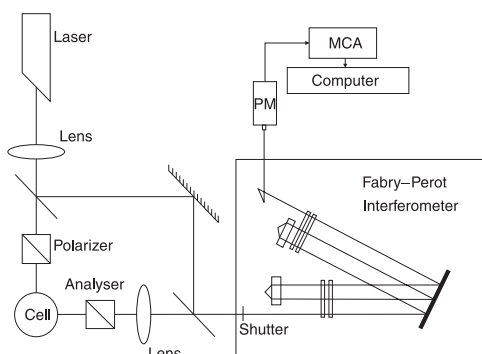
$$C(q, t) = \exp \left[-(t/\tau)^{\beta_{\text{KWW}}} \right] \quad (6)$$

with τ being the characteristic relaxation time and $0 < \beta_{\text{KWW}} \leq 1$ being the shape parameter that is a measure of the width of the distribution $L(\ln \tau)$.

Fabry–Perot Interferometry (FPI)

The fast dynamics with characteristic times from 100 ns to 1 ps, the spectrum of $C(q, t)$ (Eq. (3b)), can be recorded in the frequency domain by FPI. The six-pass tandem Fabry–Perot interferometer (Sandercock) has largely improved the versatility of the much less, compared to PCS, utilised inelastic light scattering technique. Its long-time stabilisation, the application in the presence of huge spurious elastic ($|\omega_s - \omega_i| \equiv \Delta\omega \simeq 0$) scattering and the high contrast are among the main improvements of the FP interferometry. Figure 2 shows schematically the setup where the split-off attenuated laser light is to stabilise the tandem FPI synchronised with the built-in shutter whenever complex samples display very strong elastic scattering. In case the intrinsic first-order scattering suffices for stabilisation, the quasielastic ($\Delta\omega \simeq 0$, Rayleigh spectral line) contribution is also included in the $I_{\text{is}}(q, \omega)$ spectrum.

Figure 2 Schematic experimental setup of the light scattering tandem Fabry–Perot interferometry (MCA, multichannel analyser, PM, photomultiplier tube) (Steffen *et al.*, 1993).



The current representation of the experimental spectra that is common to the quasielastic incoherent neutron scattering mimics Eq. (3b). First the instrumental (resolution) function $R(\omega)$ is fitted with a combination of Gaussian and Lorentzian functions. The known analytical Fourier transforms of these functions in the time domain, $R(t)$, are then multiplied (convolution in ω space) with the theoretical $C(q, t)$:

$$I(q, \omega) = (2\pi)^{-1} \int_{-\infty}^{+\infty} C(q, t) R(t) e^{i\omega t} dt. \quad (7)$$

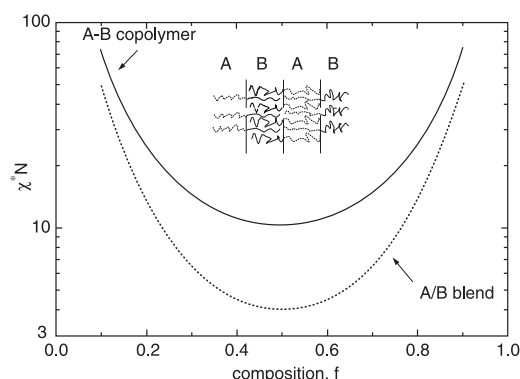
This computed spectrum is then fitted to the experimental spectra with few selected adjustable parameters, e.g., relaxation time, τ , and shape parameter β_{KWW} , for Eq. (6).

§4. Dynamic Structure Factor

Diblock Copolymers

Diblock copolymers, AB , are thermodynamically single-component systems with interacting chemically dissimilar sequences of N_A monomers A and N_B monomers B that unlike binary polymer blends, A/B , cannot macrophase separate. Instead, these fascinating systems (Bates, 1991; Fredrickson and Bates, 1996; Bates and Fredrickson, 1999;) can self-assemble in a variety of mesostructures usually with decreasing temperature below the order-to-disorder transition (ODT) and/or with increasing AB volume fraction above $\phi_{\text{ODT}}(T)$ in a common solvent for both blocks (Fredrickson and Leibler, 1989; Russel *et al.*, 1994). The phase state of a diblock is well presented (Rosedale *et al.*, 1995) in the plane $\chi^*(T, \phi)N, f$ of Fig. 3, where $\chi^*(T, \phi) \equiv \chi(T)\phi^{1.6}$ with $\chi(T)$ being the monomer–monomer van der Waals interaction, $N = N_A + N_B$ is the total polymerisation index and $f = N_A/N$ is the A composition; symmetric ($f = 0.5$) AB 's

Figure 3 Mean-field phase diagram of A/B blends (dotted line) and phase state of $A-B$ diblock copolymers (solid line). A/B become phase separate at χ^*N lower values than those of AB systems. Symmetric ($f = 0.5$) $A-B$ for $\chi^*N < 10$ are disordered and for $\chi^*N > 10$ form a lamellar microstructure schematically shown in the inset. Alternatively, symmetric A/B are miscible for $\chi^*N < 4$ and macrophase separate for $\chi^*N > 4$.



microphase separate when $\chi^*(T, \phi)N \geq 10$. Inherent to the *AB* architecture, the most probable correlation length of the composition (order parameter) fluctuations ϕ_q is a mesoscopic scale $O(R)$ (R being the polymer size). The static structure factor (all possible correlations between i and j segments on l, m polymers)

$$S(q) \equiv N^{-2} \left\langle \sum_{l,m,i,j} \exp \left[iq \left(r_l^i(0) - r_l^m(0) \right) \right] \right\rangle \quad (8)$$

should be small both at low ($qR \ll 1$) and high ($qR \gg 1$) magnification since in the former case the fluctuations are vanishingly small (very homogeneous system) while in the latter case, the scattering is dominated by correlations less than R in size with efficient local mixing of like monomers and hence low scattering intensity. $S(q)$ should therefore peak at intermediate values of q

$$S(q) \approx S(q^*) / \left[1 + (q - q^*)^2 \xi^2 \right], \quad (9)$$

where $S(q^*) \approx [F(f, q^*) - 2\chi^*N]^{-1}$, ($F(f, q^*)$ being a function of Gaussian form factors), $q^*R \approx 2$ (for $f = 0.5$) and the length ξ is a measure of the coherence of the structure characterised by the length $2\pi/q^*$; approaching ODT, $S(q)$ increases and becomes narrower. The average structure of diblock copolymers with $R < 20$ nm is well documented exclusively by X-ray and neutron scattering (Rosedale *et al.*, 1995; Koga *et al.*, 1998).

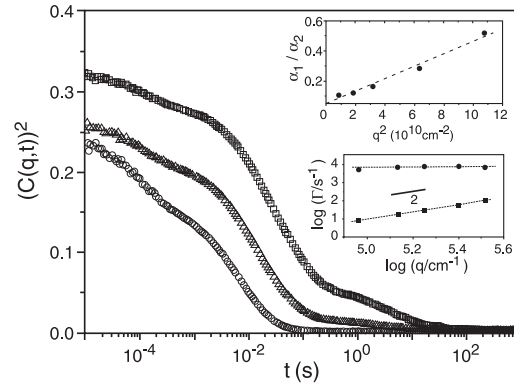
The intermediate scattering function or dynamic structure factor $S(q, t)$ (Eqs. (2) and (3) with $\delta\alpha(q, t) \propto \phi_q$) of monodisperse *AB* melts (Akcasu *et al.*, 1986; Erukhimovich and Semenov, 1986) in the random phase approximation (RPA) is a single exponential

$$S(q, t) = S(q) \exp[-\Gamma_1(q)t], \quad (10)$$

with the collective relaxation rate for the composition fluctuations (structural relaxation) $\Gamma(q) = xg(1, x)/(\tau_1 S(q))$, where $x \equiv (qR)^2$, $g(1, x) = (2x^{-2})(e^{-x} + x - 1)$ is the form factor of a single Gaussian *AB* chain (Eq. (8) for $l = m$) and τ_1 is the chain's longest relaxation time. At low magnification ($x < 1$), $g(1, x) \simeq 1$, $S(q) \propto x$ and $\Gamma_1 \approx 1/\tau_1$.

These pertinent predictions were first verified (Anastasiadis *et al.*, 1993; Vogt *et al.*, 1994) by PCS. For a poly(dimethyl-b-ethylmethylsiloxane) ($N = 1110$, $f = 0.49$) melt, the experimental $C(q, t)$ of Fig. 4 displays a fast process with both intensity and rate supporting these theoretical predictions; the N^{-3} dependence of Γ provides further support of the mechanism of the structural relaxation at low x . The second intermediate decay of $C(q, t)$ in Fig. 4 with characteristic diffusive (q^2 -dependent) rate Γ_2 and q -independent intensity S_2 (inset of Fig. 4) is at odds with Eq. (10). This new process has been identified (Jian *et al.*, 1994) as the chain self-diffusion detected due to the finite composition polydispersity

Figure 4 Polarised (VV) intensity correlation functions for a disordered poly(dimethyl-b-ethylmethyl) siloxane melt ($N = 1100$, $f = 0.49$) at 120°C at three scattering angles (\square , 45° ; \triangle , 60° ; \circ , 90°). The variation of the relaxation rates of the fast (\bullet) and intermediate (\blacksquare) processes and the amplitude ratio (a_1/a_2) of the fast chain relaxation and the chain self-diffusion with wave vector q is shown in the insets. The solid line in the lower inset indicates a slope 2 for diffusive behaviour (Anastasiadis *et al.*, 1993; Vogt *et al.*, 1994).



$\kappa_o \equiv \langle f^2 \rangle - \langle f \rangle^2$ and refractive index contrast between *A* and *B* blocks:

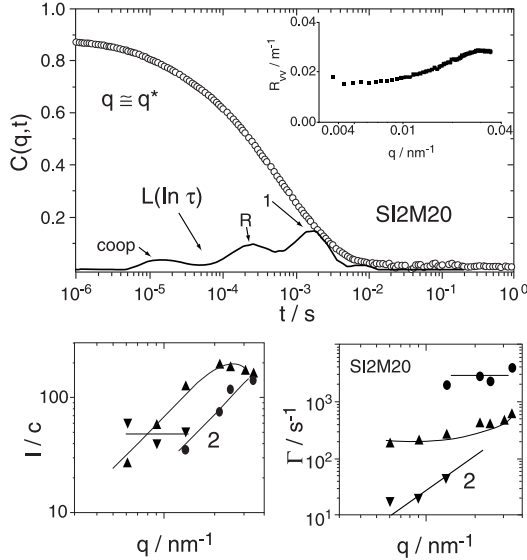
$$S_2(q, t) = S_2 \exp[-\Gamma_2(q)t] \quad (11a)$$

$$S_2 = \kappa_o q^o N / [1 - 2\chi^* N \kappa_o], \quad \Gamma_2 = D_s q^2 [1 - 2\chi^* N \kappa_o] \quad (11b)$$

The small deficiency of the best synthetic (anionic) polymerisation leads to composition heterogeneity ($\kappa_o < 0.01$) sufficient to yield the self-diffusion coefficient D_s in the low x range. The predicted divergence of S_2 for large $\chi^* N \kappa_o$ with a concurrent slowing down of Γ_2 is reminiscent of the macrophase separation of intermolecular *A/B* mixtures (Klein, 1990; Beiner *et al.*, 1998). For either melts (Anastasiadis *et al.*, 1993; Vogt *et al.*, 1994; Papadakis *et al.*, 1996; Stepanek and Lodge, 1996) or semidilute *AB* solutions (Borsali *et al.*, 1991; Duval *et al.*, 1991; Pan *et al.*, 1994; Tsunashima and Kawamata, 1994; Jian *et al.*, 1995; Molina and Freire, 1998) in common solvent, there is a consensus about the bimodal shape of $S(x, t)$ (Eqs. (10), (11)) in the low x range (long wavelength order parameter fluctuations) and the nature of the two thermal decay rates. Note that access to the two contributions to the static $S(q)$ and its additivity is possible only in a dynamic light scattering experiment. The verification of these findings for higher x values approaching x^* (≈ 2 for $f = 0.5$) would require larger sizes R (and hence molecular mass M_w). To fall into this high x range using the low light scattering q values (between 0.003 and 0.04 nm^{-1}), synthesis of *AB* with $M_w \approx O(10^6)$ is necessary.

Figure 5 shows the intermediate scattering function (Sigel *et al.*, 1999) $C(q \approx q^*, t)$ for a 2.2 wt% disordered semidilute solution of such high M_w

Figure 5 (Top) Intermediate scattering function $S(q, t)$ at $q^* \approx 0.034 \text{ nm}^{-1}$ and 25°C for 2.2 wt% SI2M20 (five times fractionated) in the common solvent toluene along with the distribution $L(\ln \tau)$ (Eq. (5)). The peaks of the latter are assigned to the cooperative diffusion (coop), and the two chain conformational motions (1 for the reptation and R for the Rouse mode). (Inset) Rayleigh ratio R_{VV} of this SI2M20 solution. (Bottom) Reduced intensities I/c (left) and relaxation rates Γ (right) associated with the composition fluctuations of different wavevectors q . \blacktriangle , \bullet , chain relaxation; and \blacktriangledown , self-diffusion. Slope 2 indicates the q^2 dependence of the intensities (I_1 and I_R) and the diffusive nature of the chain self-diffusion while the dashed lines are to guide the eye (Sigel *et al.*, 1999a).



poly(styrene-*b*-isoprene) (SI2M20) ($N = 25800$, $f_s = 0.26$), in the common solvent toluene; at 25°C this system undergoes ODT with cylindrical morphology above 7.4 wt%. The peak of $S(q)$ falls within the light scattering q values (inset of the upper part of Fig. 5) conforming to the mean-field prediction $R^{-1}(f(1-f)/3)^{-1/4}$ while the excess intensity at low q values is due to the total SI concentration fluctuations in addition to the composition polydispersity contribution S_2 (Eq. (11)). This is readily revealed by the resolution of the different contributions to the $S(q, t)$ by means of Eq. (5). Three relaxation processes were found to be the optimum solution of Eq. (5) based not only on the fit quality but also on the consistent and physically meaningful results.

The first peak of $L(\ln \tau)$ at short times relates to the cooperative diffusion responsible for the relaxation of the total AB concentration ($\phi_A + \phi_B$) fluctuations driven by the solution osmotic pressure. The location of the peak τ_c and the intensity $I_c = I(q)\alpha_c(I(q))$ is the total scattering intensity and α_c the amplitude of this process) conform to the theoretical predictions derived for semidilute solutions of linear homopolymers (de Gennes, 1979; Doi and Edwards, 1986). The other two slower processes, absent in the lat-

ter, relate to the composition fluctuation $\phi_q(t)$, and the associated reduced intensities $I_i/c \propto S_i$ and relaxation rates Γ_i are shown in the lower part of Fig. 5; the characteristics of the cooperative diffusion are not shown. The slow diffusive process in $S(q, t)$ supports the two predictions of Eq. (11) and can be therefore assigned to SI self-diffusion also confirmed by pulsed field gradient (PFG)-NMR self-diffusion data on the same sample. In the entangled concentration regime, the predicted $D_s \sim \phi^{-1.8}$ approximates well the experimental slowing down with concentration. However, the $S_2(\propto I_2/c)$ which should be virtually insensitive to ϕ variations (Eq. (11) for typical values of $\kappa_o < 0.01$) was found to increase strongly with ϕ .

The two intermediate processes between the fast cooperative and slow self-diffusion exhibit q -dependent I_i and almost q -independent rate $\Gamma_i (= 1/\tau_i)$ characteristic of chain relaxation modes. The RPA Eq. (10) for $S(q, t)$ of diblock copolymer melts is based only on Rouse dynamics (Doi and Edwards, 1986). In the presence of topological constraints (N/N_e entanglements between chains) as commonly verified by shear rheometry, $S(q, t)$ can be derived using the dynamic RPA (to include the interactions) and the two motional mechanisms for the conformational dynamics of a single chain undergoing one-dimensional curvilinear diffusion in a virtual tube of length $L_t \propto (N/N_e)$ (reptation model (Doi and Edwards, 1986)) and tube length fluctuations (Rouse model) at shorter times $\Gamma_1 t \ll 1$. In the homogeneous mean-field regime (weak thermodynamic interactions) and $x \leq x^* (\equiv (q^* R)^2)$ the two contributions read (Boudenne *et al.*, 1996, 1997)

$$S_r(q, t) \approx \left(4xNf^2(1-f^2)/\pi^4 \right) \sum_{k=0} (2k+1)^{-4} \times \exp \left[-(2k+1)^2 \Gamma_1 t \right] \quad (12a)$$

$$S_R(q, t) \approx \left(xN_e/6\pi^2 \right) \exp(-\Gamma_R t), \quad (12b)$$

where the entanglement relaxation rate $\Gamma_1 = \omega_o N_e(\phi) N^{-3} \phi^{-0.3}$, the main Rouse rate $\Gamma_R \approx \omega_o N^{-2} \phi^{-0.3}$ with $\omega_o = kT/b^2 j_o$ being the local microscopic rate (b the segment length and j_o the friction coefficient per segment) and N_e the characteristic number of monomers for entanglements. While the concentration dependence of Γ_1 (using $N_e(\phi) \sim \phi^{-0.8}$) is not far from the experimental variation, that of Γ_R is clearly weaker than experimentally found. A reduced relaxation map (Sigel *et al.*, 1999) of the different characteristic time scales of the $S(q, t)$ for SI with different molecular masses covering a wide range of reduced length scales x using exclusively experimental data is shown in Fig. 6. This plot should be valid for all diblock copolymers in the homogeneous mean field regime.

For the very high molecular mass diblocks, the ODT is approached by increasing the copolymer concentration in a common solvent at constant temper-